



## Two-stage ignition and NTC phenomenon in diesel engines



Xiao Fu, Suresh K. Aggarwal\*

Department of Mechanical and Industrial Engineering, University of Illinois at Chicago, USA

### HIGHLIGHTS

- 3-D, transient, turbulent spray simulations performed.
- Two-stage ignition in diesel sprays examined from the evolving QOOH (alkyl hydroperoxy) and OH fields.
- NTC (negative temperature coefficient) behavior investigated in sprays and homogeneous mixtures.
- Effect of methane on the ignition of n-heptane sprays in dual-fuel diesel engine characterized.

### ARTICLE INFO

#### Article history:

Received 20 August 2014

Received in revised form 15 December 2014

Accepted 16 December 2014

Available online 26 December 2014

#### Keywords:

Two-stage ignition

NTC phenomenon

Diesel spray

Dual-fuel engine

### ABSTRACT

Two-stage ignition and NTC phenomenon in diesel sprays is investigated by performing 3-D two-phase reacting flow simulations in a dual-fuel engine. Spray processes modeled include fuel atomization, droplet distortion, droplet drag, turbulent dispersion, droplet interactions in terms of collision and coalescence, vaporization, and spray-wall interaction. A validated reaction mechanism is implemented in the CFD solver, which has previously been validated for both evaporating and reacting sprays. For single-fuel cases, the effect of temperature on two-stage ignition is examined by varying the start of injection (SOI). While results indicate global similarities between the two-stage ignition processes in diesel sprays and spatially homogeneous mixtures, there are also noticeable differences between them due to temporally and spatially evolving temperature and species fields in the spray case. For instance, both the first- and second-stage ignition delays are higher for the spray cases compared to homogeneous mixtures. Second, while ignition delay for homogeneous mixtures exhibits a NTC region, that for sprays indicate a ZTC region. Moreover, the first- and second-stage ignitions for the spray occur over a wide  $\phi$  range and at multiple locations in the spray, implying a spatially wide ignition kernel. Additionally, while the chemical ignition delays are strongly influenced by the injection timing, the physical delays are essentially independent of this parameter. Results with dual fuel indicate that the two-stage ignition behavior remains intact even at high molar fractions of methane. The addition of methane increases ignition delays for both sprays and homogeneous mixtures, and can be attributed to the reduction in  $O_2$  and the chemical effect of methane. The sensitivity analysis indicated that the chemical effect is primarily due to reaction  $CH_4 + OH = CH_3 + H_2O$ .

© 2014 Published by Elsevier Ltd.

### 1. Introduction

Liquid spray combustion is employed in numerous combustion systems. Ignition represents a crucial event in the operation of these systems. Compared to a gaseous mixture, ignition in a spray is considerably more complex, as the state of ignition can be defined by three distinct ignition modes; droplet ignition, cluster ignition, and spray ignition. Ignition for an individual droplet represents the appearance of a flame near the droplet with a dimension of the order of droplet diameter. The cluster ignition refers

\* Corresponding author.

E-mail address: [ska@uic.edu](mailto:ska@uic.edu) (S.K. Aggarwal).

to the ignition around or inside a droplet cloud, while the spray ignition implies the appearance of a global flame with a dimension few orders of magnitude larger than droplet scales. In all three modes, ignition is preceded by droplet evaporation, formation of a combustible gaseous fuel-air mixture, and initiation of chemical reactions. Clearly, determination of the dominant ignition mode and the ignition behavior in each mode for different spray systems is of fundamental and practical importance [1].

Considerable research exists on these ignition modes. Aggarwal [2] and Mastorakos [3] report reviews of work dealing with laminar and turbulent spray ignition, respectively. Research on cluster ignition is discussed by Annamalai and Ryan [4], and on droplet ignition by Aggarwal [5]. As discussed in Ref. [5], numerous

experimental and computational studies concerning droplet ignition have focused on the temperature dependent chemistry effects, especially on the two-stage ignition and NTC (negative temperature coefficient) phenomenon [6–10]. Kinetics aspects of this phenomenon have been extensively studied using homogeneous mixtures [11]. As discussed in these studies, the two-stage ignition and NTC behavior is a common characteristic of the oxidation chemistry of large alkanes, described by a transition between the low- and high-temperature paths as determined by the reaction:  $R + O_2 \rightleftharpoons ROO$ . Here alkyl radical (R) is formed from fuel decomposition through H-atom abstraction. This reaction is favored below  $T \approx 800$  K, and peroxy radical then undergoes isomerization to form alkyl hydroperoxy (QOOH), which subsequently leads to the formation of ketohydroperoxide (OQOOH) and OH radicals. OQOOH being an unstable intermediate readily decomposes to form OH, alkenes and other radicals. OH then reacts with fuel to form more alkyl that feed the above chain. The above path is favored at low temperatures, leading to the first-stage ignition, characterized by a sudden but limited temperature rise. The second-stage ignition then depends upon a competition between heat releasing reactions and heat loss from the cool flame region. However, in the NTC region, the above low-temperature path becomes less important. Instead QOOH decomposes to form alkene and  $HO_2$ . In addition, alkyl radicals react to form alkenes and additional  $HO_2$ . Consequently, the ignition delay increases with the increase in temperature, as the system reactivity decreases because the branching sequence becomes less important and  $HO_2$  formation is favored compared to OH. At still higher temperatures, alkyl radicals decompose directly to form alkenes and smaller alkyl radicals through  $\beta$ -scission reactions, and the ignition process follows the high-temperature path.

While these chemistry effects are well established for homogeneous systems, they become far more complex for droplets and sprays. For droplets, additional complexity is due to the strongly coupled processes of two-phase transport, droplet heating, and vaporization. Coupling of these processes with fuel chemistry leads to multiple ignition regimes [6,7], depending upon the droplet size, fuel volatility, and ambient conditions. These regimes include (i) no ignition implying complete droplet evaporation prior to ignition, (ii) only first-stage ignition, (iii) two-stage ignition, and (iv) single-stage (hot flame) ignition. Researchers have examined these regimes through experiments using a suspended droplet, or simulations using a transient, spherically symmetric model with reduced and detailed mechanisms. The two-stage ignition was identified by following the peak temperature history, with the first temperature jump marking the first-stage ignition and the second jump representing the second-stage ignition. However, these studies did not provide a clear evidence for the NTC region, and it was surmised that the presence of non-homogeneous temperature and species fields causes a transition from the NTC to ZTC (zero temperature coefficient) region. Bouali et al. [12] suggested that competition between the availability of fuel vapor and the reduction in mixture temperature due to evaporation also plays a role. While various researchers provided different explanations for the modification of NTC behavior, only a handful of studies observed a ZTC region [6,8].

The present study has two objectives. One is to investigate the two-stage ignition and NTC phenomenon in diesel sprays. This is motivated by the consideration that ignition represents a critical process in diesel engines, and strongly influences their combustion and emission characteristics [13,14]. Moreover, new strategies, such as HCCI and LTC, for reducing engine emissions are based on controlling the ignition event. Literature review indicates that while numerous studies have investigated two-stage ignition for homogeneous mixtures and droplets, relatively little work exist for sprays [12,15]. Moreover, previous investigations have

employed simplified spray configurations, whereas the present study examines spray ignition in a diesel engine, where the ignition is influenced by the processes of fuel injection, vaporization, mixing, and kinetics. This is perhaps the first study reporting details of the first- and second-stage ignition processes by analyzing the evolution of QOOH and OH fields, as the fuel injection proceeds. Another objective is to examine the effect of methane on the two-stage ignition in diesel sprays. There is significant interest worldwide in developing NG-fueled diesel engines. However, due to its poor ignitability, a more plausible strategy is to use CI engines in a dual fuel mode with NG introduced through the intake port and diesel fuel through direct injection. Previous investigations have mostly focused on the combustion and emission characteristics of diesel engines with dual fuels [16], rather than on the ignition behavior.

## 2. Computational model

The CONVERGE 3-D software is used for simulating the fuel injection, atomization, and ignition processes in a 1.9L 4-cylinder GM light-duty diesel engine, which has been extensive used in

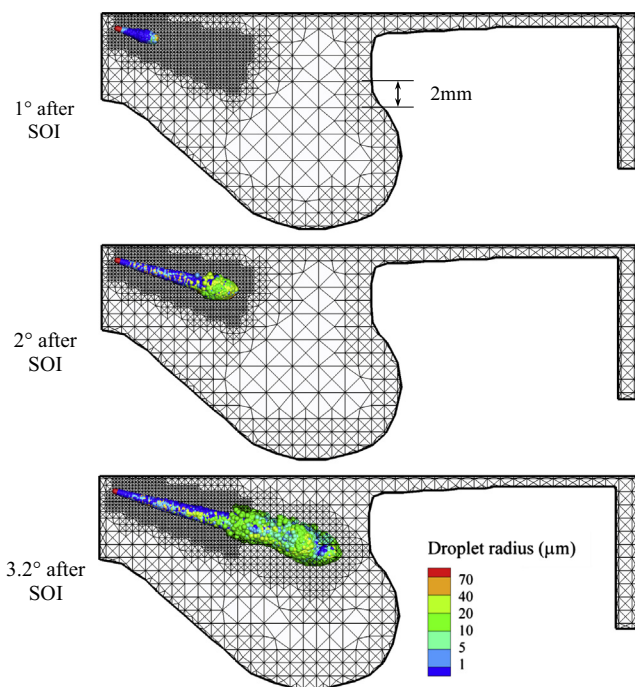


**Fig. 1.** A cross-section view of the cylinder through the spray, and the predicted spray structure for the  $-8^\circ$  SOI case at  $1^\circ$ ,  $2^\circ$  and  $3.2^\circ$  CA after SOI. Each color dot represents a droplet radius value in a given parcel, and the size distribution is indicated by the droplet radius scale ( $1$ – $70$   $\mu\text{m}$ ). The adaptive mesh evolution with time (CA) during injection and the spray development are also shown. (For interpretation of the references to color in this figure legend, the reader is referred to the web version of this article.)

**Table 1**  
Initial conditions and ignition delays in terms of crank angle for different SOIs.

SOI	$-32$	$-26$	$-20$	$-14$	$-8$	$-4$
SOI temp. (K)	700	754	812	864	903	916
SOI pres. (MPa)	1.5	2.0	2.7	3.6	4.6	5.0
$\tau_{\text{phys}}$ , physical ( $^\circ$ )	1.6	1.4	1.2	1	1	0.9
$\tau_{\text{I}}$ , 1st stage ( $^\circ$ )	13.4	9.0	5.5	3.6	2.2	2
$\tau_{\text{II}}$ , 2nd stage ( $^\circ$ )	5.2	3.8	2.8	2.2	2.4	2.5
$\tau_{\text{tot}}$ , chemical ( $^\circ$ )	18.6	12.8	8.3	5.8	4.6	4.5

experimental studies [17] at Argonne National Laboratory (ANL). It has a 7-hole common-rail injector in each cylinder. As indicated in Fig. 1, simulations consider a 1/7 (51.43°) sector of the cylinder using periodic boundary conditions at the front and back face of the sector. Details of the spray processes during injection and the adaptive grid evolution depicted in this figure are discussed later in this paper. Various engine geometry parameters are provided in Table 1 of Ref. [18]. The physical–numerical models used in the software have been described in detail elsewhere [14,19]. Therefore, only a brief summary is included here. The physical model uses a Eulerian–Lagrangian description of the two-phase turbulent reacting flow inside the cylinder. The gas-phase flow field is described using the Favre-Averaged Navier–Stokes equations along with the RNG  $k-\epsilon$  turbulence model, which includes source terms to account for the effects of discrete phase on gas-phase turbulence. A finite volume approach with a semi-implicit hybrid scheme is used to solve the gas-phase equations on a Eulerian grid. The spray is represented by a stochastic system of a discrete number of parcels, which are tracked using a Lagrangian scheme. The two phases are coupled through the mass, momentum, and energy exchange terms, which are present in both the liquid- and gas-phase equations.

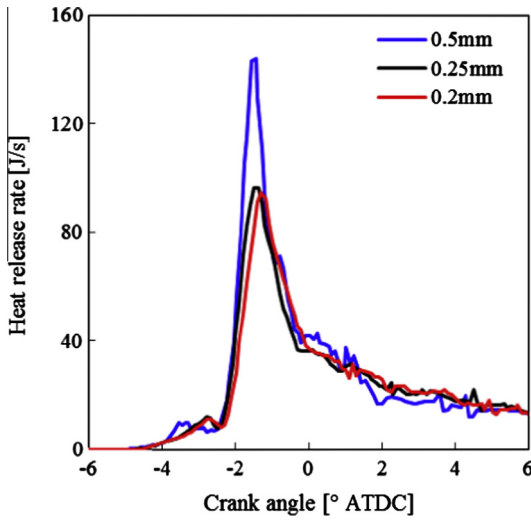


Fig. 2. Predicted heat release rate profiles for three different grid sizes for the 0% methane case with SOI = -8° ATDC.

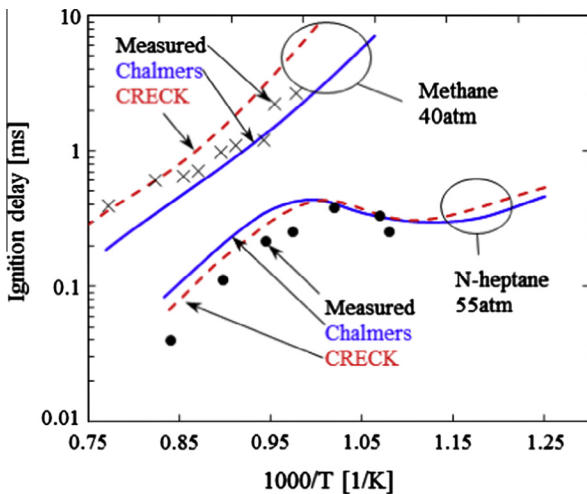


Fig. 3. Predicted and measured ignition delays for (a) n-heptane/air at  $p = 55$  atm, and (b) methane–air at  $p = 40$  atm and  $\phi = 1$ .

The length and time scales associated with the spray processes are too small to be resolved computationally, necessitating the use of sub-grid scale models to describe the spray physics. Spray processes modeled include fuel atomization, droplet distortion, droplet drag, turbulent dispersion, droplet interactions in terms of collision and coalescence, vaporization, and spray–wall interaction. The injection process is simulated using a blob injection model,

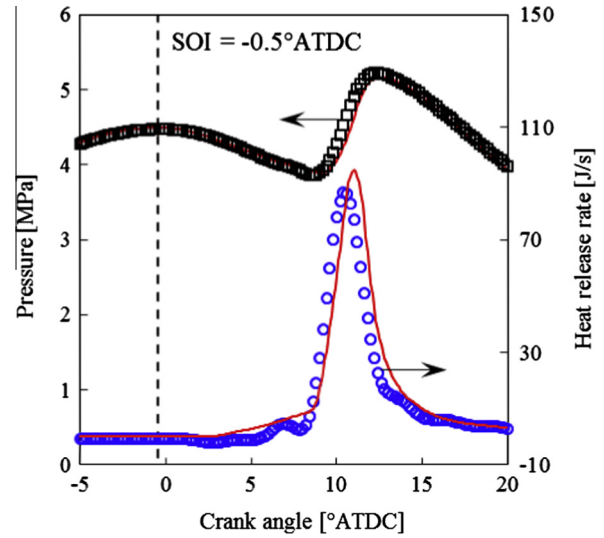


Fig. 4. Predicted and measured pressure and heat release rate profiles. Symbols represent experiment data, while lines represent predictions.

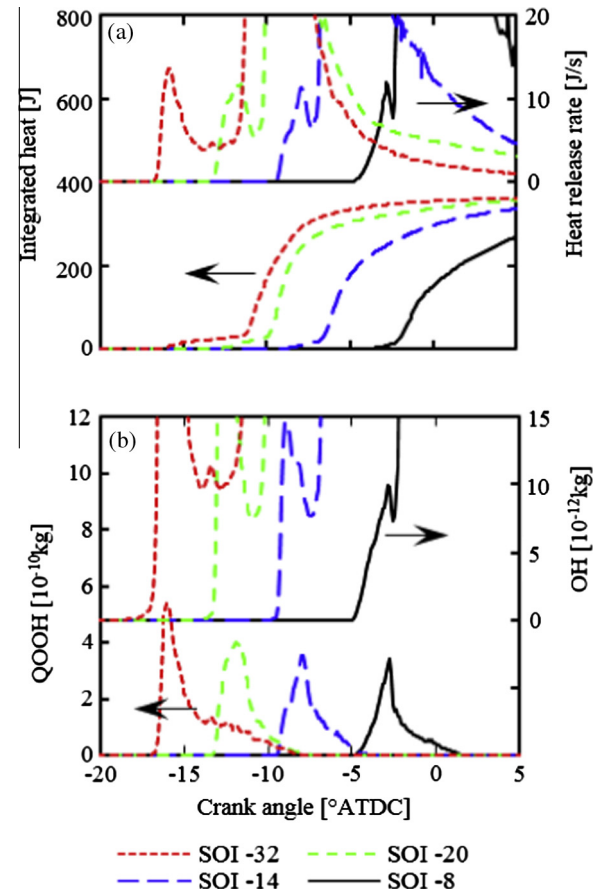


Fig. 5. HRR and IHR profiles (a), and QOOH and OH mass profiles (b) for SOI = -32, -20, -14, and -8° ATDC.

which injects liquid droplet parcels with a diameter equal to an effective nozzle diameter. The subsequent breakup process is simulated by using models based on the Kelvin–Helmholtz and Rayleigh–Taylor instabilities [20,21], while the droplet vaporization process is based on the model reported by Chiang et al. [22]. Methane and n-heptane are considered as surrogates for NG and diesel fuels, respectively. The oxidation of these fuels is modeled by incorporating the Chalmers mechanism [23], involving 42 species and 168 reactions, in the CFD solver through the SAGE chemical kinetic solver [24]. The solver uses reaction data in CHEMKIN format and computes reaction rates in each computational cell. For dual fuel cases, methane and intake air are assumed to homogeneously mixed during the intake process, while n-heptane is injected into the cylinder. For the reference case, the start of injection (SOI) is  $-8^\circ$  ATDC and injection duration is 8 CAD. The rate of injection (ROI) profile is taken from one of the experiments, corresponding to medium load condition, performed at ANL. The injection pressure was 600 bars for this condition.

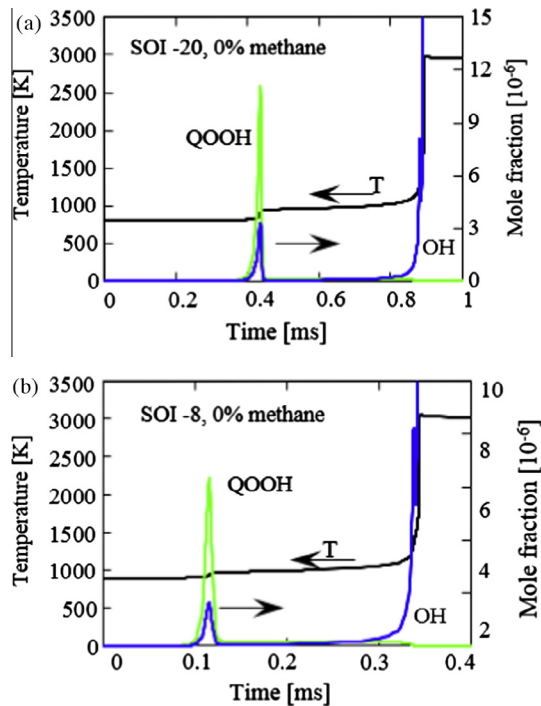


Fig. 6. Temperature, QOOH and OH mass fraction profiles for homogeneous mixtures at temperature and pressure conditions for SOI =  $-20^\circ$  and  $-8^\circ$ .

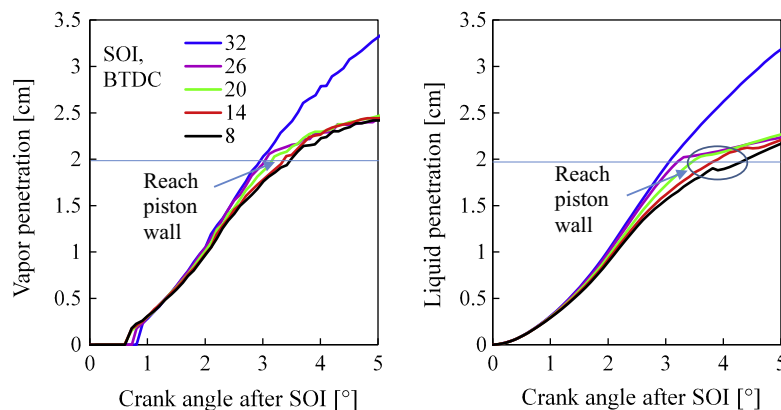


Fig. 7. Liquid and vapor penetration profiles versus crank angle after SOI for five SOI cases.

It should be noted that the turbulence combustion interaction modeling (TCI) was not considered in the present study. An appropriate TCI model will reveal more spatial details of the ignition kernel compared to the well-mixed models. However, such models are significantly more computationally expensive when implemented with detailed mechanisms in engine simulations. On the other hand, the well-mixed model has been shown to be accurate enough for predicting the basic two-phase flow properties, i.e., spray and vapor penetration, temperature profile, ignition delay, etc. Moreover, several researchers in the past have demonstrated the validity of such models for predicting combustion processes in both gasoline and compression ignition engines [25]. The issue of implementing appropriate TCI models will be examined in future work.

The CFD solver uses an innovative modified cut-cell Cartesian method for grid generation [19]. In order to resolve the flow near the injector, a local refinement region with 0.25 mm grid sizes were used, along with 0.5 mm cells for AMR (adaptive mesh resolution) based on the curvature in the velocity, temperature, and species fields. These grid sizes were determined to be sufficient to capture the spray droplet break up, vaporization, and combustion processes. This is illustrated in Fig. 2, which shows the effect of grid size on the predicted heat release rate (HRR) profiles for the SOI =  $-8^\circ$  ATDC case. As indicated, predictions with a minimum grid size of 0.25 mm are nearly grid independent. Moreover, the capability of the code for resolving high gradient regions is depicted in Fig. 1, which shows the adaptive mesh evolution with time during simulations for the reference case.

### 3. Results and discussion

The computational model used in CONVERGE has previously been validated for nonevaporating, evaporating sprays, and reacting sprays [14,18]. Validations include matching the liquid lengths, flame liftoff and flame images with the measurements of Siebers and coworkers [26,27] under diesel engine conditions. The reaction mechanism has also been validated in previous studies for the ignition of n-heptane/air mixtures at engine relevant conditions [14]. We herein provide two additional validations, one for the mechanism and the other for the engine code. Since the present work considers two fuels, validation for the ignition of n-heptane/air and methane/air homogeneous mixtures at elevated pressures is presented in Fig. 3. Simulations in a constant pressure homogeneous reactor using the Chalmers mechanism are compared with the measurements of Gauthier et al. [28] and Huang et al. [29], and the predictions of a more comprehensive and extensively validated CRECK mechanism with 466 species 14,631 reactions [30].

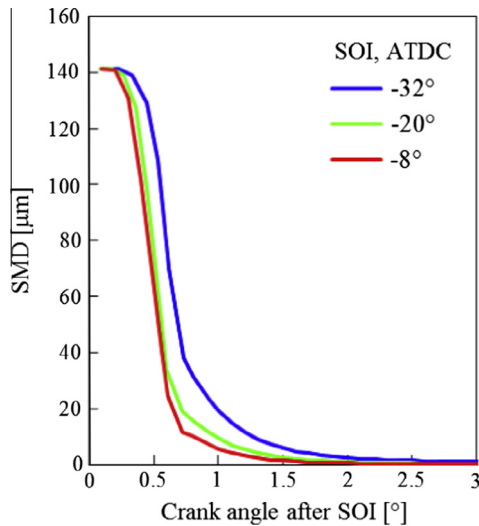


Fig. 8. Sauter Mean Diameter (SMD) vs. crank angle after SOI for the three SOI cases.

Overall, there is good agreement between the measurements and simulations, with the Chalmers mechanism somewhat overpredicting ignition delays for n-heptane and underpredicting for methane at high temperatures. The mechanism also captures the two-stage ignition and NTC behavior, which is the focus of the present study.

Additional validation for engine simulations is provided using the pressure and heat release rate data from ANL for the same engine [17]. Fig. 4 presents a comparison of the predicted and measured heat release rate and pressure profiles with respect to the crank angle. For these results, the SOI is  $-0.5^\circ$  ATDC and injection duration is 8 CAD. There is good overall agreement between the predictions and measurements, especially with respect to pressure profiles. There are some differences for the HRR profiles, with the computational model slightly overpredicting the HRR values.

### 3.1. Two-stage ignition in diesel sprays

Results focus on the two-stage ignition phenomenon for both the single and dual fuel cases. The effect of initial temperature is characterized by varying the SOI from  $-32^\circ$  to  $-4^\circ$  ATDC. Fig. 5 presents heat release rate (HHR), integrated heat release (IHR), QOOH and OH mass profiles with respect to crank angle. Note that in diesel engines, it is difficult to vary initial temperature independent of pressure, since both increase as SOI is delayed during the compression stroke (cf. Table 1). Also, as indicated in the table, the initial temperature is considered in the range in which the two-stage ignition and NTC behavior is of interest. The first- and second-stage ignition delays ( $\tau_I$  and  $\tau_{II}$ ) can be determined from the HHR or IHR profile. For instance, CA at which IHR exceeds 0.01 J is used to define the first ignition, while the inflection point in IHR profile defines the second ignition. These ignition delays are consistent with those determined from the QOOH and OH profiles, where the first inflection point in QOOH, indicating the sharp rise, yields  $\tau_I$  and the second rise (after the first peak) in OH yields  $\tau_{II}$ . The corresponding plots for homogeneous mixtures for two SOIs are shown in Fig. 6. The first, second, and total chemical ignition delays ( $\tau_{tot} = \tau_I + \tau_{II}$ ), and the physical delay for the four SOIs are also listed in Table 1. The physical delay is defined as the time (CA) between the start of injection and when the n-heptane fuel vapor mass exceeds  $10^{-8}$  kg. As indicated in the table, the physical delay is relatively insensitive to SOI. This aspect was further analyzed by examining the fuel atomization and vaporization characteristics.

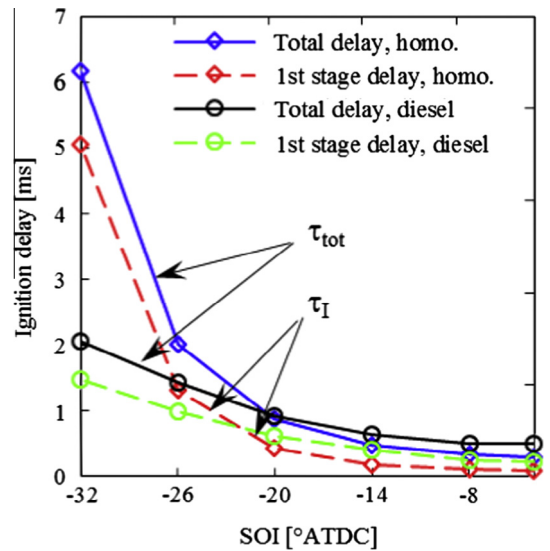


Fig. 9. First and total ignition delays versus SOI for the homogeneous mixture and diesel spray.

Fig. 7 presents the integrated liquid and vapor penetration profiles for different SOIs. Except for the  $SOI = -32^\circ$  case, for which the liquid spray impinges on the piston wall (crown region), the penetration profiles exhibit similar behavior, except that as the SOI is advanced, the liquid and spray penetrations are increased due to lower ambient density. Moreover, the physical delay for these cases is less than  $2^\circ$  CA (Table 1), and during this period, the penetration behavior is essentially identical for all five SOIs. This is further illustrated by the temporal evolution of SMD (Sauter Mean Diameter) presented in Fig. 8 for three different SOIs. As the SOI is advanced, the decrease in SMD becomes slower. This is mainly due to the slower vaporization process at lower mixture temperatures with advanced injection. However, a more important observation is that within  $2^\circ$  CA after injection, the SMD values become quite small and nearly independent of SOI, implying that the physical delay is not much affected by the SOI in the present study.

The comparison of ignition delays for the diesel spray and homogeneous mixture (Table 1) indicates that while both  $\tau_I$  and  $\tau_{II}$  decrease as SOI is delayed, the effect is stronger on  $\tau_I$ , which is consistent with previous droplet studies [6,7], indicating that the initial temperature has a stronger effect on  $\tau_I$ . Fig. 9 compares the first and total ignition delays for the homogeneous mixture and engine spray. Simulations for homogeneous cases were performed at the same initial pressure and temperature as those for the diesel

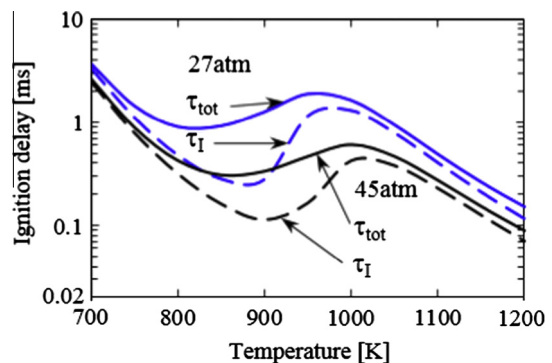
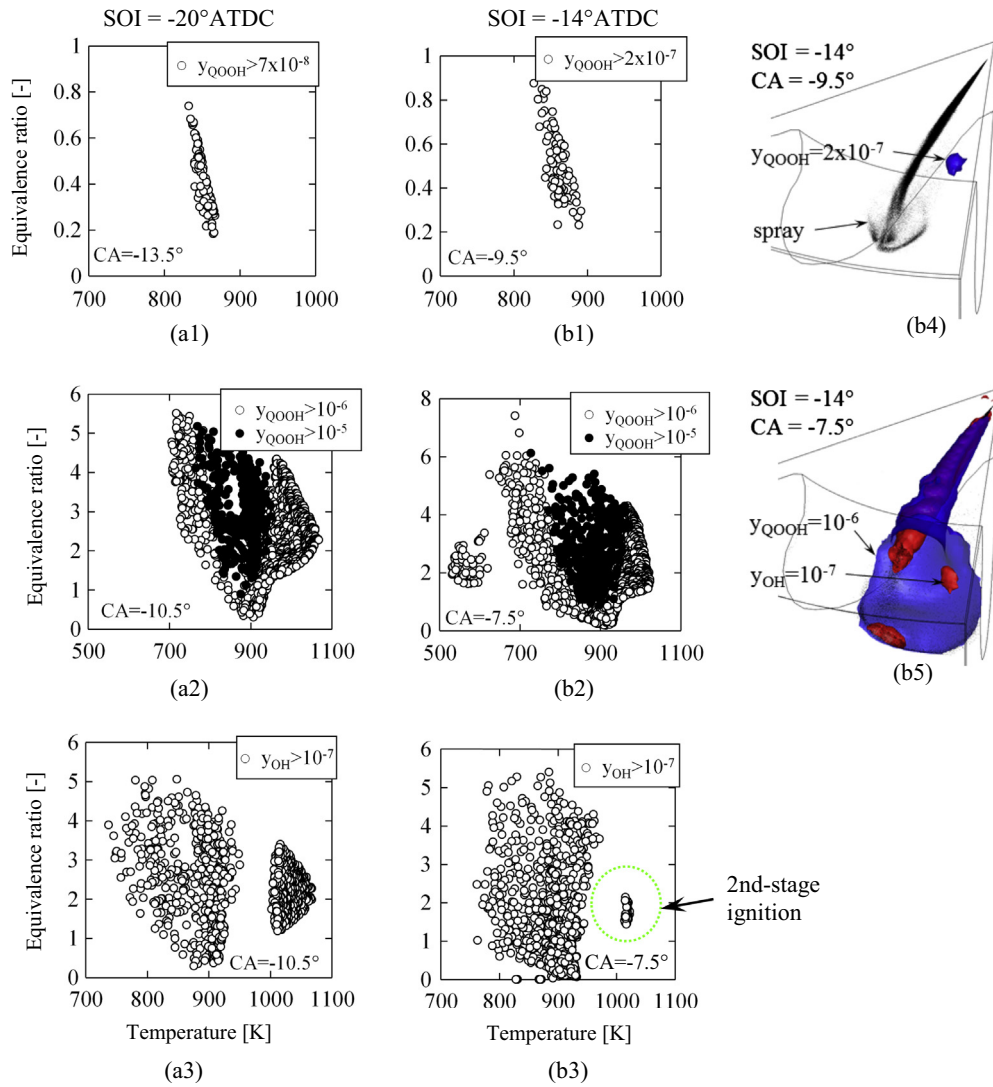


Fig. 10. First and total ignition delays versus temperature for homogeneous mixture at  $p = 27$  and 45 atm.



**Fig. 11.** First and second stage ignition processes depicted through the scatter plots in  $\phi$ - $T$  space, and contour plots (in physical space) of QOOH and OH mass fraction for the  $-20^\circ$  and  $-14^\circ$  SOIs. QOOH scatter plots are at crank angles near first and second ignition, while OH plots are near second ignition. QOOH and OH contour plots in Fig. 8b4 and b5 show the first- and second-stage ignition kernels in physical space for the  $-14^\circ$  SOI case.

spray. For these conditions, the ignition delay plots for both the homogeneous mixture and spray cases indicate a nearly ZTC region rather than a NTC region. Note that as SOI is varied from  $-20^\circ$  to  $-8^\circ$ , the temperature increases from 812 K to 903 K. However, this also increases the pressure from 27 to 45 atm, and the absence of NTC region may be due to this effect. This is confirmed by Fig. 10, which plots ignition delays versus temperature at different pressures for homogeneous mixtures. As pressure increases, it decreases both the first and total ignition delays, and thus smoothen the NTC region.

Results in Figs. 5–9 indicate significant differences between the ignition processes in homogeneous systems and diesel sprays. First of all, ignition delays exhibit stronger sensitivity to temperature for the homogeneous case compared to that for the spray. This is related to the vaporization and other two-phase flow effects, which smoothen out the temperature effect. Second, while in both cases, the first ignition is characterized by RO2 isomerization and subsequent formation and consumption of QOOH (cf. Figs. 5 and 6), it is also strongly influenced by the temporally and spatially evolving temperature and species fields for the spray case. These effects are evident from the fact that QOOH and OH radicals continue to form (cf. Fig. 5) during and after the first stage ignition in the spray case.

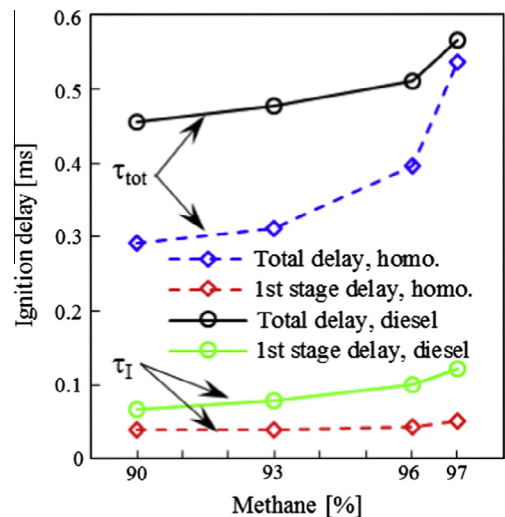


**Fig. 12.** First and total ignition delays versus methane molar fraction for homogeneous system and diesel spray.

The two-phase flow effects and the evolution of the first and second ignition kernels are seen more clearly in shown in Fig. 11, which presents scatter and iso-contour plots of QOOH and OH mass fraction for the  $-20^\circ$  and  $-14^\circ$  SOIs.<sup>1</sup> The scatter plots are shown in  $\varphi$ - $T$  space, where the local  $\varphi$  is based on n-heptane fuel vapor, and contour plots (Fig. 11a4 and a5) are in the physical space. The first- and second-stage ignition processes are generally similar for the two SOIs, except for differences in the ignition delay values. For both cases, QOOH plots (Fig. 11a1 and b1) indicate that the first ignition occurs over a relatively narrow  $T$  range ( $\approx 850$  K), but a wide  $\varphi$  range (0.3–0.8), implying a spatially wide ignition kernel. The temperature and species fields then continue to evolve due to vaporization, mixing and chemical reactions. This is illustrated by the broadening of QOOH (Fig. 11a2 and b2) and OH (Fig. 11a3 and b3) scatter plots, and by increasing  $\varphi$  and  $T$  values. The temperature increases due to heat release from the first ignition, which in turn enhances vaporization rate and promotes ignition kinetics leading to second-stage ignition, which occurs near  $T \approx 1025$  K, but over a wide  $\varphi$  range between 1 and 3. This is clearly indicated by the second OH scatter plot near  $\varphi \approx 2$  and  $T \approx 1025$  K in Fig. 11a3 and b3. Thus, processes leading to second ignition are also strongly influenced by the spatially and temporally evolving two-phase flow field in engines, whereas in homogeneous systems, it essentially depends on temperature at the end of first stage. Furthermore, the first and second ignition locations are spatially separated in engine sprays, as illustrated by QOOH and OH contour plots in Fig. 11b4 and b5 for the SOI =  $-14^\circ$  case. The QOOH contour plots in Fig. 11b4 indicate that the first ignition kernel develops outside the main spray, since the mixture inside the spray is too rich to ignite for this case. In addition, the OH contours in Fig. 11b5 indicate the existence of multiple ignition kernels both inside and outside the spray.

### 3.2. Effect of methane on two-stage ignition

Results in this section examine the effect of methane on two-stage ignition in diesel sprays and homogeneous mixtures. Engine simulations were performed at SOI =  $-8^\circ$  with constant n-heptane mass, but varying the amount of methane in the cylinder. Note that cases with only high mole fractions of  $\text{CH}_4$  are relevant, since for lower  $\text{CH}_4$  mole fractions the ignition behavior is mostly controlled by n-heptane ignition chemistry. Simulations for homogeneous cases were performed at the same pressure and temperature as those for the engine. Fig. 12 compares the first and total ignition delays for diesel sprays and homogeneous mixtures for different methane molar fractions. Note that as the amount of methane is increased, it decreases the amount of air or  $\text{O}_2$  in the mixture. This also increases the engine power, which in fact represents a viable approach for operating a dual-fuel engine at different loads. Important observations from Fig. 12 are:

- (i) Both the first ignition and total ignition delays are higher for the spray compared to those for homogeneous mixture, which again can be attributed to the spatially and temporally evolving two-phase flow. As stated earlier,  $t_1$  and  $t_{11}$  can be determined from the QOOH and OH profiles, which are shown in Fig. 13 for both the homogeneous mixtures and sprays.
- (ii) The two-phase flow effects for spray ignition can be seen in Fig. 14, which presents the QOOH and OH scatter plots in  $\varphi$ - $T$  space for the 97% methane case. Similar to the 100% n-heptane case (cf. Fig. 11), the QOOH scatter plot at  $-5.2^\circ$  ATDC indicates that the first-stage ignition occurs over a

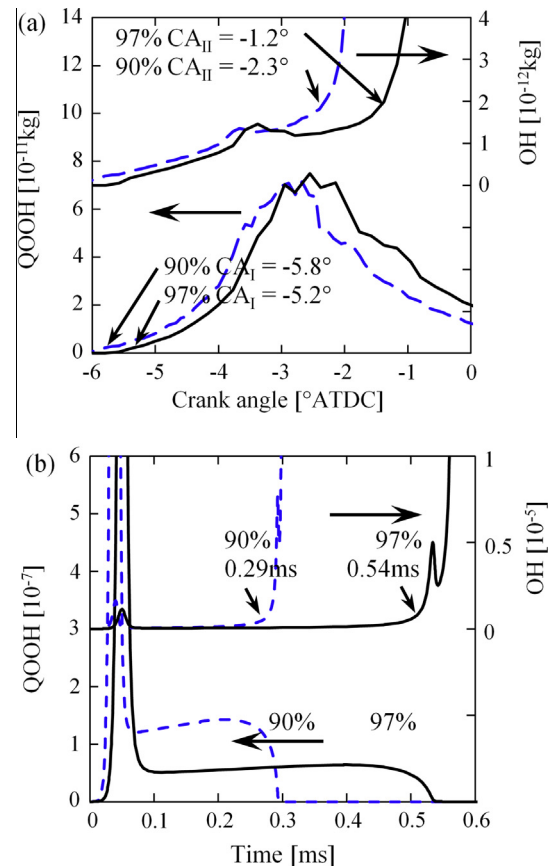
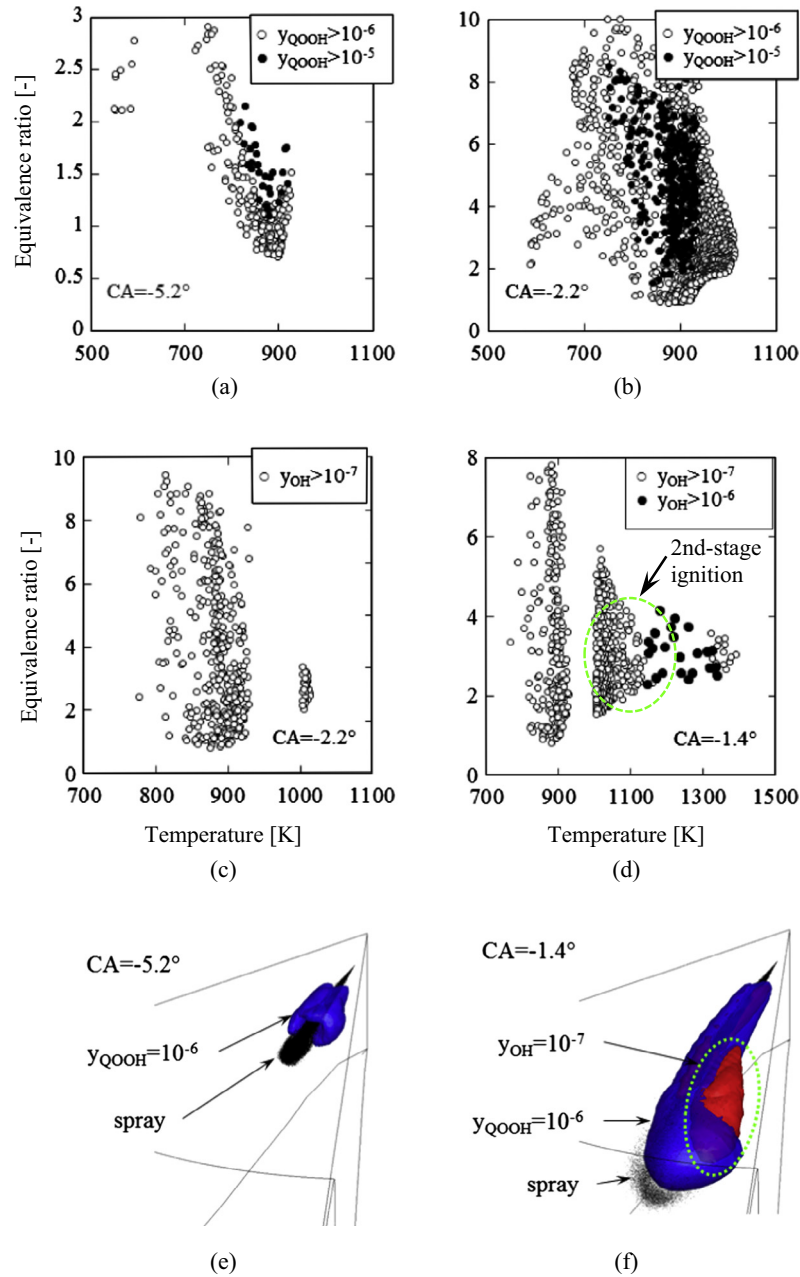


Fig. 13. QOOH and OH mass profiles during ignition of diesel spray (a) and QOOH and OH mole fraction profiles for homogeneous mixture (b) for 90% and 97% methane.

relatively narrow  $T$  range ( $\approx 850$  K) but a wide  $\varphi$  range ( $\varphi = 1$ – $2$ ). Subsequently the temperature increase due to first ignition enhances the vaporization rate and promotes ignition kinetics leading to second-stage ignition, which occurs near  $-1.4^\circ$  ATDC. The second-stage ignition again occurs over a narrow  $T$  range ( $\approx 1050$  K) but a wide  $\varphi$  range (2–4), as indicated by the OH scatter plots in Fig. 14c and d. The QOOH and OH contour plots in Fig. 14e and f indicate significantly different physical locations for the first- and second-stage ignition kernels. More importantly, the plots in Figs. 11 and 14 seem to indicate that the spray ignition processes are qualitatively similar for the single-fuel (100% n-heptane) and dual-fuel cases, implying that the overall two-stage ignition behavior remains intact even at very high methane fractions, and is determined by n-heptane chemistry. However, the  $\varphi$  range and physical locations of the first- and second-stage ignition kernels are noticeably influenced by methane.

- (iii) For both the homogeneous mixture and spray,  $t_1$  and  $t_{11}$  increase as the amount of methane is increased. The increase in  $t_1$  is primarily due to a reduction in  $\text{O}_2$ , which decreases the RO2 and QOOH concentrations. In contrast, the increase in  $t_{11}$  may be attributed to both the reduction in  $\text{O}_2$  and the chemical effect of methane on ignition kinetics. Moreover the presence of methane has a more pronounced effect on  $t_{11}$  compared to that on  $t_1$ , which is another indication of its chemical effect. The sensitivity analysis (not shown here) indicated that the inhibiting effect of methane is primarily due to reaction  $\text{CH}_4 + \text{OH} = \text{CH}_3 + \text{H}_2\text{O}$ , which depletes OH radicals.

<sup>1</sup> A video file is provided as supplementary material, showing details of the spray and temporal evolution of the two-stage ignition processes in terms of evolving QOOH and OH fields.



**Fig. 14.** Spray ignition process depicted through the scatter and contour plots of QOOH and OH mass fraction for the 97% methane case with SOI =  $-8^\circ$  ATDC. QOOH scatter plots are shown at the first ignition ( $-5.2^\circ$ ) and before the second ignition ( $-2.2^\circ$ ), while OH scatter plots are before ( $-2.2^\circ$ ) and at second ignition ( $-1.4^\circ$ ). QOOH and OH contours in Fig. 11e and f indicate the first- and second-stage ignition kernels in physical space, respectively.

#### 4. Conclusions

3-D simulations were performed to examine the two-stage ignition and NTC phenomenon in diesel sprays. The temporal and spatial behavior of the first- and second-stage ignition processes was analyzed from the evolution of QOOH (alkyl hydroperoxy) and OH fields, respectively in both  $\phi$ - $T$  space and physical space. The effect of temperature was characterized by varying the start of injection (SOI). As SOI is delayed, the cylinder temperature increases, and, consequently, both the first- and second-stage ignition delays decrease, but the effect is stronger on the first-stage ignition, which is consistent with previous droplet theory.

While results indicate global similarities between the two-stage ignition processes in diesel sprays and spatially homogeneous gaseous mixtures, there are also significant differences due to the

temporally and spatially evolving temperature and species fields in the spray case. Ignition delays for homogeneous mixtures exhibit a NTC region, while those for sprays indicate a near ZTC region. The transition from NTC to ZTC behavior for diesel sprays is mainly due to the evolving two-phase flow, and also partly due to the increase of pressure during the compression stroke. In addition, the first- and second-stage ignitions for the spray occur over a wide  $\phi$  range, implying a spatially wide ignition kernel. Moreover, depending upon the operating conditions, multiple ignition kernels are observed in diesel sprays. Results further indicate that while the chemical ignition delays are strongly influenced by the SOI, the physical delays are essentially independent of this parameter.

Results for the dual-fuel cases indicate that the two-stage ignition behavior remains intact even at high molar fractions of methane. The addition of methane increases ignition delays for both

sprays and homogeneous mixtures, and can be attributed to the reduction in  $O_2$  and the chemical effect of methane. Reaction  $CH_4 + OH = CH_3 + H_2O$  was found to be primarily responsible for the chemical effect.

## Appendix A. Supplementary material

Supplementary data associated with this article can be found, in the online version, at <http://dx.doi.org/10.1016/j.fuel.2014.12.059>.

## References

- [1] Chiu HH, Kim HY, Croke EJ. Internal group combustion of liquid droplets. *Proc Combust Inst* 1982;19(1):971–80.
- [2] Aggarwal SK. A review of spray ignition phenomenon: present status and future research. *Prog Energy Combust Sci* 1998;24:565–600.
- [3] Mastorakos E. Ignition of turbulent non-premixed flames. *Prog Energy Combust Sci* 2009;35:57–97.
- [4] Annamalai K, Ryan W. Interactive processes in gasification and combustion. Part I: liquid drop arrays and clouds. *Prog Energy Combust Sci* 1992;18:221–95.
- [5] Aggarwal SK. Single droplet ignition: theoretical analyses and experimental findings. *Prog Energy Combust Sci* 2014. <http://dx.doi.org/10.1016/j.pecs.2014.05.002>.
- [6] Tanabe M, Bolik T, Eigenbrod C, Rath HJ, Sato J, Kono M. Spontaneous ignition of liquid droplets from a view of non-homogeneous mixture formation and transient chemical reactions. *Proc Combust Inst* 1996;26:1637–43.
- [7] Moriue O, Eigenbrod C, Rath HJ, Sato J, Okai K, Tsue M, et al. Effects of dilution by aromatic hydrocarbons on staged ignition behavior of n-decane droplets. *Proc Combust Inst* 2000;28:969–75.
- [8] Schnaubelt S, Moriue O, Coordest T, Eigenbrod C, Rath HJ. Detailed numerical simulations of the multistage self-ignition process of n-heptane, isolated droplets and their verification by comparison with microgravity experiments. *Proc Combust Inst* 2000;28:953–60.
- [9] Cuoci A, Mehl M, Buzzi-Ferraris G, Faravelli T, Manca D, Ranzi E. Autoignition and burning rates of fuel droplets under microgravity. *Combust Flame* 2005;143:211–26.
- [10] Stauch R, Lipp S, Maas U. Detailed numerical simulations of the autoignition of single n-heptane droplets in air. *Combust Flame* 2006;145:533–42.
- [11] Curran HJ, Pitz WJ, Westbrook CK, Callahan CV, Dryer FL. Oxidation of automotive primary reference fuels at elevated pressures. *Proc Combust Inst* 1998;27:379–87.
- [12] Bouali Z, Pera C, Reveillon J. Numerical analysis of the influence of two-phase flow mass and heat transfer on n-heptane autoignition. *Combust Flame* 2012;159:2056–68.
- [13] Pickett LM, Kook S, Persson H, Andersson O. Diesel fuel jet lift-off stabilization in the presence of laser-induced plasma ignition. *Proc Combust Inst* 2009;32:2793–800.
- [14] Som S, Aggarwal SK. Effects of primary breakup modeling on spray and combustion characteristics of compression ignition engines. *Combust Flame* 2010;157:1179–93.
- [15] Wolff MC, Meisl J, Koch R, Wittig S. The influence of evaporation on the autoignition-delay of n-heptane air mixtures under gas turbine conditions. *Proc Combust Inst* 1998;27:2025–31.
- [16] Korakianitis T, Namasivayam AM, Crookes RJ. Natural-gas fueled spark-ignition (SI) and compression-ignition (CI) engine performance and emissions. *Prog Energy Combust Sci* 2011;37:89–112.
- [17] Ciatti S, Subramanian SN. An experimental investigation of low-octane gasoline in diesel engines. *J Eng Gas Turbines Power* 2011;133:092802-1–092802-11.
- [18] Aggarwal SK, Longman DE. A computational study on the effects of pre-ignition processes on diesel engine combustion and emissions. *AJTEC* 2011–44202, *Proc ASME/JSM E 8th thermal engineering joint conference*; 2011.
- [19] Richards KJ, Senecal PK, Pomraning E. CONVERGE (Version 2.1.0), Convergent Science Inc., Middleton, WI; 2013.
- [20] Reitz RD, Diwakar R. Structure of high pressure sprays. *SAE Trans* 1987;96:492–509.
- [21] Patterson MA, Reitz RD. Modeling the effects of fuel spray characteristics on diesel engine combustion and emission, SAE Technical Paper; 1998. 980131.
- [22] Chiang CH, Raju MS, Sirignano WA. Numerical analysis of convecting, vaporizing fuel droplet with variable properties. *Int J Heat Mass Transfer* 1992;35:1307.
- [23] <http://www.tfd.chalmers.se/~valeri/MECH.html>.
- [24] Senecal PK, Pomraning E, Richards KJ, Briggs T, et al. Multi-dimensional modeling of direct-injection diesel spray liquid length and flame lift-off length using CFD and parallel detailed chemistry. SAE Technical Paper; 2003-01-1043.
- [25] <http://www.sandia.gov/ecn/workshop/ECN2.php>.
- [26] Siebers DL, Higgins B. Flame lift-off on direct-injection diesel sprays under quiescent conditions. SAE Technical Paper; 2001-01-0530.
- [27] Higgins B, Siebers DL. Measurement of the flame lift-off location on di diesel sprays using oh chemiluminescence. SAE Technical Paper; 2001-01-0918.
- [28] Gauthier BM, Davidson DF, Hanson RK. Shock tube determination of ignition delay times in full-blend and surrogate fuel mixtures. *Combust Flame* 2004;139:300–11.
- [29] Huang J, Bushe WK, Hill PG, Munshi SR. Experimental and kinetic study of shock initiated ignition in homogeneous methane–hydrogen–air mixtures at engine-relevant conditions. *Int J Chem Kinet* 2006;38:221–33.
- [30] C1C16 Low and High Temperature, Version 1212, December 2012. <<http://creckmodeling.chem.polimi.it/index.php/current-version-december-2012/c1c16-low-and-high-temperature>>, (accessed in 2013).